Capability of LEPS Surfaces to Describe the Kinetics and Dynamics of Non-Collinear Reactions

J. Espinosa-García*

Departamento de Química Física, Universidad de Extremadura, 06071 Badajoz, Spain

Received: May 8, 2000; In Final Form: September 22, 2000

The popular LEPS surface for collinear reaction paths and a simple bent surface yielding a nonlinear saddle point geometry were used to examine the capability of the LEPS surfaces in describing the kinetics and dynamics of systems with noncollinear reaction paths. The parameters calculated for the atom−diatom Cl + ClH reaction include geometries, vibrational frequencies, and curvatures (to estimate the tunneling effect) along the reaction path, as well as variational transition-state theory rate constants and kinetic isotope effects. The collinear LEPS and the bent surfaces for this triatomic system show similar behavior, so similar behavior in noncollinear polyatomic reactions may be expected, with the consequence of saving time and computational effort.

I. Introduction

The potential energy surface (PES) of London, Eyring, and Polanyi, modified later by Sato and denoted the LEPS surface,[1,2] has been widely used for the kinetic and dynamic study of triatomic systems and, with suitable modifications, as a starting point for more complex polyatomic systems. In this latter case, we can speak of a LEPS-type surface to distinguish it from the "pure" LEPS surface used for triatomic systems. Its main advantage is that since it has been so widely used, it is a well-tested and well-calibrated surface, but its main disadvantages are that it produces a collinear saddle point geometry and does not consider realistic long-range wells.

In the study of hydrogen abstraction reactions, many systems evolve with a collinear (or quasi) saddle point geometry, and our group, among others, has used this LEPS-type surface[3−10] as the basis for building a complete surface of polyatomic systems which correctly represents the stretching and bending modes while saving computation time. When the reaction exhibits a small separation of the linearity, as for example in the CH_4 + F reaction,[3] we also used this type of surface with reasonable results for the kinetics and dynamics. However, there are some systems (although comparatively few), such as Cl +ClH or NH_3 + O(^{3}P), that involve nonlinear saddle point geometries with central angles in the range of 135−170°, depending on the calculation level. For these systems, there arises the question of whether the popular and simple LEPS-type surface can describe a nonlinear system? In the present work, the atom−diatom Cl + ClH system and its deuterated analogue are used as tests.

The Cl(^{2}P) + HCl($^1\Sigma^+$) → HCl($^1\Sigma^+$) + Cl(^{2}P) reaction has received much attention in last years as prototype of reactions with heavy−light−heavy mass combinations, and it is a good candidate for large tunneling effect. Although a recent ab initio study[11] at a multiconfigurational level has described the three lowest PESs of the system ($1^2A'$, $2^2A'$, and $1^2A''$ symmetry), we focus here on the ground-state surface ($2^2A'$ symmetry), which contributes about 90% to the rate constant.

Potential energy surface calculations for this system have been reported with different methods, using ab initio electronic structure methods[11−18] and semiempirical LEPS-type surfaces.[19−21] With respect to the LEPS surfaces, we would emphasize the Bondi−Connor−Manz−Römelt (BCMR) surface[19] and the PK1, PK2, and PK3 surfaces of Persky and Kornweitz.[20] The PK1 surface is similar to that of BCMR, while the other two are only identical to that of BCMR for collinear geometries and have higher bending frequencies. Using high-level ab initio calculations,[13,15] the collinear barrier height is predicted to be in the range of 8.3−10.7 kcal mol^{-1}, in accordance with the 8.6 kcal mol^{-1} recommended by Kneba and Wolfrum.[22] For the nonlinear saddle point geometry (bent structure),[13,15,17] the barrier height is in the range of 5.9−10.0 kcal mol^{-1}, with a central angle (Cl−H−Cl) between 136° and 161°, depending on the level of calculation. When comparison is possible[13,15] at the same level of calculation, the bent geometry is 1.0−1.5 kcal mol^{-1} more stable than that of the collinear. Some authors[13,17,23] have used ab initio information in order to produce potential energy surfaces. Thus, Garrett et al.[13] used POLCI ab initio calculations for geometries near those of collinear ClHCl and later scaled this information to reproduce experimental rate data (denoted as s-POLCI surface), obtaining a nonlinear saddle point (161.4°). Schatz et al.[23] noted that this surface was not a global surface and proposed fitting the earlier data for ClHCl angles greater than 150° (sf-POLCI denotes scaled and fitted POLCI surface). Using quantum scattering calculations, these authors concluded that the nonlinear saddle point obtained with the sf-POLCI surface does not strongly change the dynamics relative to the linear saddle point of the BCMR surface, although this comparison should be taken with caution and more theoretical or experimental studies could be necessary. However, using canonical variational transition-state theory (CVT) with tunneling correction, Garrett and Truhlar[24] later found significant kinetic changes between the collinear BCMR and the bent sf-POLCI surfaces, with the rate constants differing by factors of 1.8−1.3 in the temperature range of 312.5−423.2 K. A detailed analysis of this final result shows that the difference is

* E-mail: joaquin@unex.es.

10.1021/jp001729x CCC: $20.00
Published on Web 12/08/2000

TABLE 1: Surface Parameters[a] for the Cl + ClH Reaction

	BCMR[b]		S1[c]		S2[d]	
parameter	ClH	ClCl	ClH	ClCl	ClH	ClCl
D_e (kcal mol^{-1})	106.477	57.983	106.551	57.997	106.551	56.997
R_e (Å)	1.275	1.988	1.275	1.988	1.275	2.208
β (Å^{-1})	1.868	2.002	1.867	2.062	1.867	2.022
Sato, Δ	0.115	0.115	0.115	0.115	0.176	0.176
K_{eq} (mdyne Å rad^{-2})			1.006		1.006	
α (Å^{-1})			1.110		1.010	
θ° (rad)			2.7925		2.8925	

[a] The definition of the parameters for the BCMR are standard (see, for example, ref 1). [b] Ref 19. [c] S1 is the bent PES from this work with a barrier height of 8.6 kcal mol^{-1} for direct comparison with the collinear BCMR surface. [d] S2 is the bent PES from this work fitted to reproduce the experimental H-transfer rate constants.

due to the CVT values, while the tunneling factor (a dynamic feature) is similar for the two surfaces. Recently, González et al.[17] proposed an analytical expression based on a many-body expansion using 740 ab initio calculations; they obtained a more bent saddle point (141.06°) and compared the CVT/tunneling results with those from the BCMR surface. These authors found similar final rate constants for both surfaces (as a consequence of the calibration process imposed) but different individual contributions. Thus, while the CVT values are similar, the tunneling factors are very different. For example, at 300 K, the fitted PES gives 1.13, while the BCMR gives 15.48, i.e., about 14 times larger, due to the different shape of the reaction path. Note that these results run contrary to Garrett and Truhlar's. Finally, the tunneling factor affects the kinetic isotope effect, whose value is 3.87 for the fitted PES and 9.08 for the BCMR (experimental value of 9.35 from González et al.).

In summary, from reviewing the literature, we conclude that the description of many points using high-level calculations to produce analytical surfaces is an expensive process and does not guarantee the quality of the final result. Therefore, given the intrinsic interest of using a simple functional form such the LEPS surface and given the economy involved in avoiding the computational description of the surface, this present paper analyzes the capability of LEPS-type surfaces in describing the kinetics and dynamics of systems with bent saddle point geometries, first for a triatomic system and then as a projection of future polyatomic system applications. The paper is organized as follows. Section II presents the original BCMR parameters for the collinear saddle point and the new functional form designed to describe the bent saddle point geometry. The computational details describing the reaction-path analysis, variational transition-state theory (VTST), and tunneling methods are also included. The results of VTST calculations are presented in Section III and compared to accurate quantum mechanical and experimental values. This section also contains a comparison of the predictions from the new surface with the experimental kinetic isotope effects (KIEs). Finally, the conclusions are presented in Section IV.

II. Methods and Computational Details

A. Potential Energy Surface. For the symmetric linear saddle point, we use the BCMR surface,[19] which is a LEPS surface with the parameters given in Table 1. Basicaly, the LEPS functional form involves a singlet curve dependent on four parameters ($^1D_{X-Y}$, R_{X-Y}, β_{X-Y} and S_{X-Y}) for each X−Y bond.

To take into account the deviation from linearity (180°), we augment this BCMR surface with a harmonic bending term (V_{harm}) to describe the Cl−H−Cl bending mode

$$V_{harm} = {}^1/_2K(\theta - \theta^\circ)^2 \tag{1}$$

where θ° is the equilibrium angle of Cl−H−Cl at the saddle point ($\theta^\circ \neq 180^\circ$ and it is defined later) and the ClHCl angle is defined as

$$\theta = \cos^{-1}[(R_{ClH}{}^2 + R_{HCl}{}^2 - R_{ClCl}{}^2)/2R_{ClH}R_{HCl}] \tag{2}$$

To provide the correct asymptotic values, we attenuated the force constant, K, using the following switching function:

$$K = K_{eq}\{1 - \tanh[\alpha(R_{ClCl} - R_{ClCl}{}^\circ)]\} \tag{3}$$

where K_{eq} and α are adjustable parameters for reproducing the bending frequency at the bent saddle point geometry. Therefore, the new PES function is

$$V = V_{LEPS} + V_{harm} \tag{4}$$

Note that this model potential is not symmetric; i.e., it does not satisfy the condition $V(\pi - \phi) = V(\pi + \phi)$, where ϕ measures the deviation from linearity. However, since there is a deep well around the equilibrium angle θ° (in fact, $V(\pi) - V(\theta^o) > K_BT$, where K_B is the Boltzmann's constant and T the temperature), this simple potential is adequate for describing the main goal of this work, i.e., the linear/bent saddle point comparison. Clearly, this asymmetric behavior is an inconvenient feature when the PES is used for trajectory calculations, and more complex functional forms are necessary, as for example a quadratic-quartic expression. The latter, however, lies beyond the scope of this manuscript.

Having fixed on the functional form, we calibrated the new PES, and in this work, we have used two criteria, each with its particular objective. In the first case, the PES is calibrated to reproduce the barrier height of the linear BCMR surface to make a more direct comparison between the two surfaces. This surface is denoted as S1. Thus, the only modification, apart from the three new parameters of the V_{harm} term, is in the β_{Cl-Cl} paramater. In the second case, we use the reproduction of the experimental H-transfer rate constants as calibration criterion. This surface is denoted as S2. We change the three parameters of the V_{harm} term, all the parameters of the Cl−Cl bond, and the Sato parameter of the Cl−H bonds. All parameters used in these calibrations are listed in Table 1.

The results of the final fits appear in Table 2 for the saddle point, together with other theoretical estimates for comparison. The bent S1 surface, used in this work for direct comparison with the collinear BCMR surface, correctly reproduces the geometry, frequency, and energies of the BCMR surface. The two degenerate bending frequencies (508 cm^{-1}) of the BCMR surface are thus reproduced by one bending frequency (960 cm^{-1}) on the S1 surface, and therefore, the adiabatic barrier heights are practically equivalent. The bent S2 surface, used in this work to reproduce the experimental H-transfer rate constants, presents a good agreement (geometry, frequency, and energies) with other ab initio surfaces, such as the scaled and fitted ab initio POLCI surface[13,23] (sf-POLCI), which is also a bent surface (161.4°).

B. Computational Details. The minimum energy path (MEP) is calculated using the Page and McIver method[25] with a step size $s = 0.0001$ amu$^{1/2}$ bohr ($s > 0$ refers to the product side). In the rest of paper, the units of s will be bohr, and all calculations will be carried out in mass-scaled coordinates with a

TABLE 2: Comparison of Saddle Point Properties for Some Cl + ClH(D) Surfaces

	surface				
	collinear		noncollinear		
property[a]	BCMR	sf-POLCI	sf-POLCI	S1[b]	S2[b]
R(ClH)	1.467	1.473	1.473	1.469	1.473
∠ClHCl	180.0	180.0	161.4	166.6	168.4
$\Delta E^{\ddagger}$	8.55	9.01	7.52	8.60	7.10
harmonic frequencies					
H isotope					
sym. stretch	344	336	326	311	341
bend	508	1118 i	1617	960	1436
	508	1118 i			
antisym. stretch	1398 i	1627 i	1606 i	1406 i	1500 i
D isotope					
sym.stretch	344	336	326	307	340
bend	362	812 i	1152	693	1024
	362	812 i			
antisym. stretch	996 i	1159 i	1145 i	1002 i	1068 i
V_aG					
H isotope	10.50		9.73	10.42	9.64
D isotope	10.03		9.25	10.03	9.05

[a] Distance in Å, angles in deg, frequency in cm^{-1}, and energies in kcal mol^{-1}. $\Delta E^{\ddagger}$ stands for the classical barrier energy and V_aG the vibrationally adiabatic ground-state potential barrier, i.e., $\Delta E^{\ddagger}$ + zero-point energy. [b] S1 is the PES from this work with $\Delta E^{\ddagger} = 8.60$ kcal mol^{-1} for comparison with the collinear BCMR surface, and S2 is the PES from this work fitted to reproduce the experimental H abstraction rate constants.

reduced mass μ equal to 1 amu. Thus, distances through the mass-scaled coordinates in bohr are equivalent to distances through mass-weighted coordinates in $amu^{1/2}$ bohr. We calculated the reaction path between $s = -4.0$ and $+4.0$ bohr. Along the MEP, a generalized normal-mode analysis was performed[26] using a curvilinear projection operator[27] formalism. With this information, we calculated first the ground-state vibrationally adiabatic potential curve

$$V_aG(s) = V_{MEP}(s) + \epsilon_{int}G(s) \quad (5)$$

where $V_{MEP}(s)$ is the classical energy along the MEP with its zero energy at the reactants $s = -\infty$ and $\epsilon_{int}G(s)$ is the zero-point energy at s from the generalized normal-mode vibrations orthogonal to the reaction coordinate. Second, we calculated the coupling term, $B_{k,F}(s)$, measuring the coupling between the normal mode k and the motion along the reaction coordinate, mode F. The $B_{k,F}(s)$ coupling terms are the components of the reaction-path curvature, $\kappa(s)$, defined as

$$\kappa(s) = (\sum[B_{k,F}(s)]^2)^{1/2} \quad (6)$$

and control the nonadiabatic flow of energy between these modes and the reaction coordinate.[28] The interest in the calculation of these coupling terms lies in the qualitative explanation of the possible vibrational excitation of reactants and/or products, i.e., dynamical features.

Finally, the energies, vibrational frequencies, geometries, and gradients along the MEP were used to estimate rate constants and kinetic isotope effects (KIEs) by using variational transition-state theory (VTST). We calculated thermal rates using the canonical variational theory[29,30] (CVT) approach, which locates the dividing surface between reactants and products at a point $s_*^{CVT}(T)$ along the reaction path that minimizes the generalized TST rate constants, $k^{GT}(T,s)$ for a given temperature T.

In the present work, we used the ABCRATE[31] and POLYRATE[32] programs. The ABCRATE code calculates rate constants for atom−diatom reactions with collinear reaction paths only, but it permits the simultaneous calculation of anharmonicity, curvilinear coordinates, and large-curvature tunneling. The POLYRATE code is a general polyatomic rate constants code, which permits collinear and bent reactions but no simultaneous calculation of the three aforementioned factors. The rotational partition functions were calculated classically, and vibrations were treated as quantum mechanical separable harmonic oscillators, with the generalized normal modes defined in curvilinear coordinates.[27,33,34] The advantage of curvilinear coordinates (nonlinear functions of Cartesian coordinates) over rectilinear ones (linear functions of Cartesian coordinates) is that in some cases the lowest bending frequencies had unphysical imaginary values over a wide range of the reaction coordinate using rectilinear coordinates, whereas these frequencies were real over the whole of the reaction path using curvilinear coordinates, as has been confirmed in the title reaction and other hydrogen abstraction reactions.[5,7,9] The anharmonicity is included as implemented in the ABCRATE code; i.e., stretch anharmonicity was treated by the WKB method,[35] and the bending anharmonicity was included in an uncoupled-mode approximation using a quadratic-quartic potential.[36] Also, we included the $^2P_{1/2}$ excited state of Cl in the reactant electronic partition function (882 cm^{-1}). Finally, we considered the tunneling contributions. Since the heavy−light−heavy mass combination is present in this hydrogen-transfer reaction, a large curvature tunneling (LCT) calculation is necessary. We used the microcanonical optimized multidimensional tunneling (μOMT) approach[37] in which, at each total energy, the larger of the semiclassical tunneling corrections of the small-curvature (CD-SCSAG)[38] and large-curvature (LCG3)[30] approximations is taken as the best estimate.

III. Results and Discussion

We begin by comparing the results of the kinetics and dynamics for the collinear BCMR and the bent S1 surfaces, which display (from the calibration criterion) similar shapes and barrier heights.

A. Reaction Path and Frequency Analysis. Classical energies along the MEP, V_{MEP}, and ground-state vibrationally adiabatic potential energy curves, ΔV_aG, as a function of s are plotted in Figure 1 for the BCMR and S1 surfaces. The V_{MEP} is practically the same for the two surfaces (only one is plotted), while the ΔV_aG curves show small differences, with a symmetric double well around the saddle point.

Figure 2 plots the variation of the broken (Cl−H) and formed (H−Cl) bonds during the reaction as a function of s. Both BCMR and S1 surfaces exhibit similar behavior, and only the S1 results are plotted. As the reaction proceeds, the Cl−H bond remains practically constant until the reaction coordinate reaches about −0.40 bohr, where it starts changing almost linearly with s. A symmetric change is also observed for the H−Cl forming bond, at $s = +0.40$ bohr. The points where these changes take place show the beginning of the dissociation and the end of the formation of the Cl−H bonds, and their location is related to the largest changes of the vibrational frequencies and to the reaction-path curvature, as will be analyzed below (Figures 3 and 4).

The vibrational frequencies along the MEP are shown in Figure 3 for the BCMR (dashed line) and S1 (solid line) surfaces. The most important change corresponds to the evolution of the Cl−H symmetric stretching mode from reactants to products. This mode drops dramatically near the saddle point ($s = 0$). The fall and subsequent rise in its frequency are located

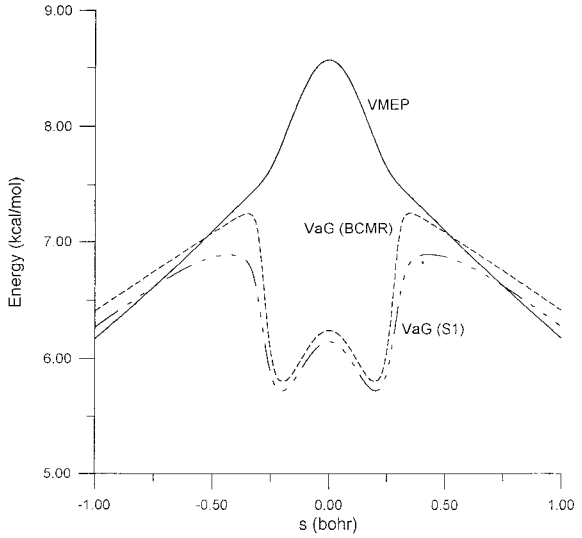

Figure 1. Classical potential energy curve, V_{MEP}, and vibrationally adiabatic potential energy curves, ΔV_aG, as a function of reaction coordinate s for the collinear BCMR and bent S1 surfaces. All quantities are with respect to the reactants.

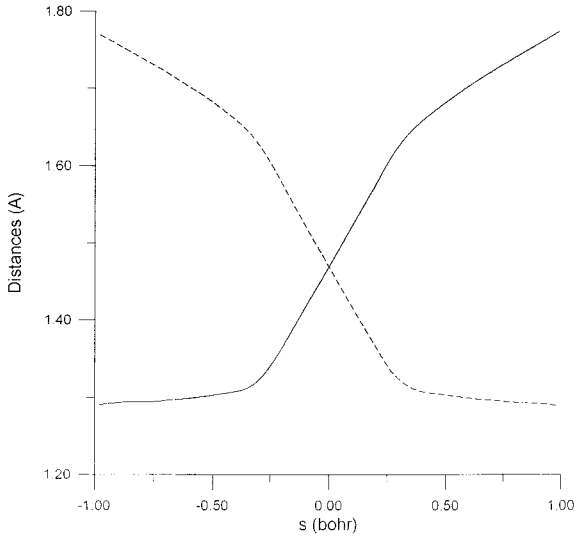

Figure 2. Cl−H bond distance as a function of the reaction coordinate s. Note that $s = 0$ corresponds to the saddle point.

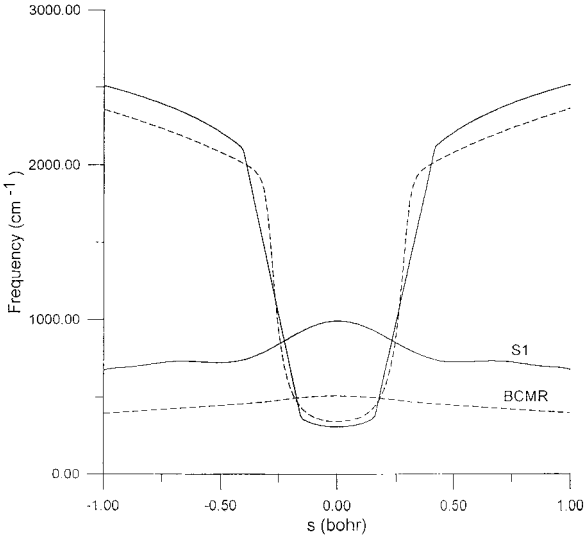

Figure 3. Generalized normal-mode vibrational frequencies plotted vs the reaction coordinate for the BCMR (dashed line) and S1 (solid line) surfaces. The lowest frequencies for the BCMR surface correspond to a doubly degenerate value.

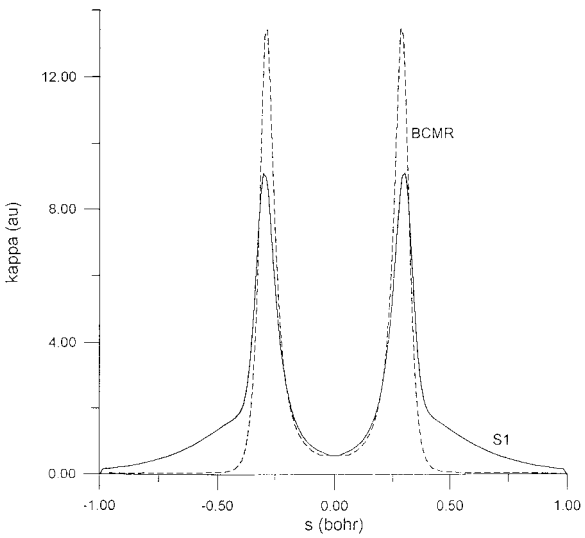

Figure 4. Reaction-path curvature (κ) as a function of s for the BCMR (dashed line) and S1(solid line) surfaces.

at approximately the same points where the Cl−H bond is broken and formed, respectively, i.e., where these distances reach a value almost equal to their asymptotic limits (Figure 2). The lowest frequencies (bending modes, one for the S1 surface and two degenerate modes for the BCMR surface) appear along the reaction path as a consequence of the transformation of free rotations and translations at the reactant and product limits into real vibrational motions in the triatomic system. It is interesting to note that the two surfaces show similar behavior for both symmetric stretching and bending modes.

Further analyzing the reaction valley, we plot the curvature term (κ) of the reaction path as a function of s in Figure 4 for the BCMR (dashed line) and S1 (solid line) surfaces. The two surfaces display similar behavior, with two symmetric sharp peaks due to strong coupling with the Cl−H stretch mode in the reactant and product channels. Both surfaces have two maxima at about $s = -0.30$ and $+0.30$ b, but the peaks are larger for the BCMR surface. This analysis provides 2-fold information. It shows first that the reaction-path curvature must be taken into account in order to calculate the tunneling effect and, second, illustrates the nonadiabatic flow of energy between this mode and the reaction coordinate. The large coupling for the Cl−H stretching mode indicates that excitation of this mode would greatly enhance the reaction rates (entry channel) and that excitation of this mode can be expected for thermal reactions (exit channel).

B. Rate Constants for the Isotopically Unsubstituted Reaction. Continuing with the BCMR and S1 comparison, the analysis of the ΔV_aG curves (Figure 1) showed the existence of three maxima, two of equal height separated by one with a lower maximum, and therefore, the rate constants were finally calculated using the canonical unified statistical model (CUS).[30]

Table 3 lists the variational CVT/μOMT and CUS/μOMT rate constants for the BCMR and S1 surfaces, together with the three-dimensional quantum calculations using the centrifugal sudden distorted-wave (CSDW) method[39] on the BCMR surface, which are the best available quantal results for this surface.

First, we consider the H-transfer reaction on the BCMR surface. With the anharmonic approximation, the CVT/μOMT values agree with the earlier results of Garrett and Truhlar[24] and are smaller than the CSDW values by a factor of 1.64−

TABLE 3: Rate Constants[a] for the Cl + ClH Reaction with a Barrier Height around 8.6 kcal mol^{-1}

	S1 surface[b]		BCMR surface[b]		BCMR surface[c]		BCMR[d]
T (K)	CVT/μOMT	CUS/μOMT	CVT/μOMT	CUS/μOMT	CVT/μOMT	CUS/μOMT	CSDW
312.5	4.26(−16)[e]	2.17(−16)	7.40(−16)	3.87(−16)	7.91(−16)	6.17(−16)	1.3(−15)
358.	1.33(−15)	6.92(−16)	2.16(−15)	1.15(−15)	2.43(−15)	1.90(−15)	-
368.2	1.66(−15)	8.65(−16)	2.66(−15)	1.42(−15)	3.02(−15)	2.36(−15)	5.6(−15)
423.2	4.52(−15)	2.43(−15)	6.93(−15)	3.76(−15)	8.35(−15)	6.48(−15)	1.6(−14)

[a] In cm^3 molecule^{-1} s^{-1}. [b] Vibrational harmonic approximation and curvilinear coordinates. [c] Vibrational anharmonic approximation and curvilinear coordinates. [d] Three-dimensional quantum calculation using the centrifugal sudden distorted-wave (CSDW) method from ref 39. [e] 4.26(−16) stands for 4.26×10^{-16}.

TABLE 4: Rate Constants[a] for the Cl + ClH Reaction on the S2 Surface

T (K)	CUS/μOMT[b]	CSDW[c]	exp.[d]
312.5	1.95(−15)	1.5(−15)	1.5 ± 0.8(−15)
358.	4.44(−15)		4.2 ± 2.5(−15)
368.2	5.20(−15)	7.3(−15)	5.1 ± 2.4(−15)
423.2	1.07(−14)	2.4(−14)	1.5 ± 0.6(−14)

[a] In cm^3 molecule^{-1} s^{-1}. [b] This work, on the S2 surface. [c] Ref 39 on the sf-POLCI surface. [d] Refs 22, 40, and 41, as reanalyzed in ref 13.

TABLE 5: Kinetic Isotope Effects for the Cl + ClH(D) Reaction on Several Surfaces

	CUS/μOMT[a]		CUS/μOMT[b]		ICVT/		
T (K)	BCMR	S1	harm.[c]	anharm.[d]	LCG3[e]	CSDW[f]	exp.[g]
312.5	5.11	3.81	5.14	6.42	4.66	15.46	8.6 ± 1.1
358.	4.08	3.31	4.18	5.22			
368.2	3.90	3.18	4.02	5.02	3.66	10.90	5.0 ± 0.7
423.2	3.18	2.62	3.85	4.81	3.14	8.57	4.1 ± 0.4

[a] This work with vibrational harmonic approximation. [b] This work on the S2 surface. [c] Vibrational harmonic approximation for H and D transfer. [d] Vibrational anharmonic estimate using the anharmonic correction from the BCMR collinear surface (see text). [e] Ref 24 on the sf-POLCI surface. [f] Ref 39 on the sf-POLCI surface. [g] Ref 13.

1.91 in the temperature range of 312.5−423.2 K. However, with the CUS approach (factor not considered in earlier variational work[24]), the rate constants diminish with respect to the CVT values by a factor of 1.28 over all the temperature range (recrossing effect), and therefore, the differences with respect to the CSDW become larger. With the harmonic approximation, which will be used for direct comparison with our S1 results, the CVT/μOMT values agree with the anharmonic results, but the CUS/μOMT values are smaller. Therefore, the CUS approximation is more sensitive to the harmonic/anharmonic vibrational mode description.

If the bent S1 surface is now considered with the harmonic approximation, both the CVT/μOMT and the CUS/μOMT rate constants will be smaller than those using the BCMR surface. For example, the CUS/μOMT difference at 312.5 K is due to the tunneling effect (decreasing by a factor of 3.42) and the CUS rate constant (increasing by a factor of 1.92). However, it is encouraging that the two surfaces show a similar behavior of the rate constants with temperature, although the only calibration criterion used for the S1 surface was to reproduce the BCMR barrier height.

For comparison purposes, and in light of the poor agreement obtained with the bent S1 surface (as could be expected from the restricted calibration criterion imposed), we re-fitted the surface's parameters to reproduce the experimental rate constants. The Cl + ClH reaction has been the object of few experimental work,[22,40,41] reanalyzed by Garret et al.,[13] over the temperature range of 312.5−423.2 K, with an estimated activation energy of 5.5 ± (0.2−2.5) kcal mol^{-1}, which, as can be seen, presents a large error bar. We thereby obtained the bent S2 surface. The activation energy for the temperature range of 312.5−423.2 K is 4.03 kcal mol^{-1}, within the range of the experimental estimates. Table 4 lists the CUS/μOMT rate constants for this surface. The results are compared with the CSDW quantum calculations[39] on the bent sf-POLCI surface, the best available quantal results for this bent surface, which test the quality of the empirical surface (obviously, this comparison is not totally exact because the surfaces are not the same, but it permits a good estimate).

Our results show relative agreement with the CSDW quantum calculations, with higher values at low temperature and lower values at high temperature, and both within the experimental error bar. The cause of this discrepancy may be (i) the different surfaces (S2 and sf-POLCI), (ii) the different methods (variational and CSDW), (iii) the different treatment of the anharmonicity, or (iv) a combination of these factors.

Similar differences (or even larger) were found when the semiclassical variational theory,[24] and the CSDW quantum[39] calculations were compared on the same sf-POLCI surface (this eliminates possibility i). When the bending vibrations are treated as uncoupled, discrepancies of 1.1 (312.5 K) and 2.2 (423.2 K) are found, while when the effect of coupling the bending vibrations is included, these differences increase (2.4 at 312.5 K and 4.2 at 423.2 K). Garrett and Truhlar[24] concluded that the difficulty of making accurate semiclassical predictions is associated more with the unusually large anharmonicity for this surface than with the nature of the tunneling process per se.

C. Kinetic Isotope Effects. To complete the comparison of the collinear BCMR/bent S1 surfaces, we shall calculate the KIEs, which provide a very sensitive test of several features of the shape of the surface (barrier height and width and zero-point energy near the dynamic bottleneck). The Cl + ClH/Cl + ClD KIEs are listed in Table 5 for the temperature range of 312.5−423.2 K. When the harmonic approximation are used for both cases, the two surfaces show a similar behavior with temperature, with values lower than the experimental data, especially at low temperature. Note that the S1 KIEs are the smaller; although given the very restricted calibration criterion, these values are not disappointing.

Finally, to complete the test of the new S2 surface, we shall calculate the KIEs, which also appear in Table 5. Our results with the harmonic approximation (fourth column) agree with the experimental values within their uncertainties, except at the lowest temperature, where the value is underestimated. However, for this triatomic system on the sf-POLCI surface, Garrett and Truhlar[24] demonstrated that the anharmonicity and the vibration−rotation coupling are very important. In fact, we indirectly considered these effects in our surface because the calibration process was performed to reproduce the H-transfer rate constants (which already include these effects). Nevertheless, the vibrational frequencies of the deuterated analogue are smaller (a flatter curve), and therefore, the anharmonicity will affect the unsubstituted and the deuterated compounds differently and will

be reflected in the KIE values. Those authors demonstrated that the vibration−rotation coupling affects H and D compounds practically to the same extent (see Tables 5 and 6 of ref 24) and will therefore practically not affect the KIEs. With respect to the anharmonicity, unfortunately no data are available on a bent surface for the harmonic/anharmonic comparison, and we estimated this effect by using a collinear system (BCMR surface using the ABCRATE code, which permits, as we mentioned above, the simultaneous calculation of anharmonicity, curvilinear coordinates, and large-curvature tunneling). In the temperature range analyzed, the estimated anharmonic effect increases the KIEs by 1.25 on average. However, Cohen et al.,[18] using the semiclassical transition-state theory (STST), found no significant harmonic/anharmonic differences in the common temperature range, although they concluded pessimistically: "All of this discussion makes it difficult to say anything conclusive about the reliability of the calculated STST rates for ClH and ClD reactions". The fifth column of Table 5 shows the harmonic KIEs with the anharmonic correction estimated in this work. The estimated anharmonic KIEs show better agreement with the available experimental data, taking into account the experimental uncertainties. The CSDW quantal[39] and the ICVT/LCG3 variational[24] results overestimate and underestimate, respectively, this magnitude over the entire temperature range. We think that these KIEs lend confidence to the very simple functional form (quadratic function) used in the present paper.

IV. Conclusions

The present study has examined whether the popular LEPS surface can be used to describe the kinetics and dynamics of systems with noncollinear reaction paths. Using the atom−diatom Cl + ClH system as test, we compared the results for the kinetics and dynamics for a typical collinear LEPS surface (BCMR) with those for a simple bent surface constructed and calibrated in this work. We found that the breaking/forming bonds, the maximum change in the stretching mode, the reaction-path curvature (an important factor related to the tunneling effect and the reaction coordinate-bound modes coupling), the rate constants, and the KIEs over the common temperature range behave similarly for the two surfaces, taking into account the calibration criterion. This capability of the typical LEPS surface to reproduce the kinetics and dynamics of triatomic systems with noncollinear reaction paths, which agrees with the conclusion of Schatz et al.[23] using a different bent surface, is encouraging and opens up the possibility of using this simple functional form as a starting point in constructing analytical potential energy surfaces for noncollinear polyatomic systems. It represents a great savings in calculation time, since it is well-known that the complete construction of an analytical surface of polyatomic reactions is no trivial task and is very time-consuming. Work with noncollinear polyatomic systems is in progress in our laboratory to check this hypothesis.

Acknowledgment. The author is very grateful to Dr. J. C. Corchado for many helpful discussions and computational efforts, and he acknowledges one of the reviewers for the useful comments on the symmetry of the bending harmonic term. This work is supported in part by Consejería de Educación, Ciencia y Tecnología, Junta de Extremadura (Spain) (Project IPR99A009), and Ministerio de Educación y Ciencia (Spain) (Project PB98-0998).

References and Notes

(1) Johnston, H. S. *Gas-Phase Reaction Rate Theory*; Ronald Press: New York, 1966; p 119.
(2) Smith, I. W. M. *Kinetics and Dynamics of Elementary Gas Reactions*: Buttherwoths, London, 1980.
(3) Corchado, J. C.; Espinosa-García, J. *J. Chem. Phys*. **1996**, *105*, 3160.
(4) Espinosa-García, J.; Corchado, J. C. *J. Chem. Phys*. **1996**, *105*, 3517.
(5) Corchado, J. C.; Espinosa-García, J. *J. Chem. Phys*. **1997**, *106*, 4013.
(6) Espinosa-García, J.; Corchado, J. C. *J. Phys. Chem. A* **1997**, *101*, 7336.
(7) Corchado, J. C.; Espinosa-García, J.; Roberto-Neto, O.; Chang Y. Y.; Truhlar, D. G. *J. Phys. Chem. A* **1998**, *102*, 4899.
(8) Espinosa-García, J.; Sansón, J.; Corchado, J. C. *J. Chem. Phys.* **1998**, *109*, 466.
(9) Espinosa-García, J. *J. Chem. Phys*. **1999**, *111*, 9330.
(10) Espinosa-García, J.; Corchado, J. C. *J. Chem. Phys*. **2000**, *112*, 5731.
(11) Maierle, C. S.; Schatz, G. C.; Gordon, M. S.; McCobe, P.; Connor, J. N. L. *J. Chem. Soc., Faraday Trans*. **1997**, *93*, 709.
(12) Botschwina, P.; Mayer, W. *Chem. Phys. Lett*. **1976**, *44*, 449.
(13) Garrett, B. C.; Truhlar, D. G.; Wagner, A. F.; Dunning, T. H. *J. Chem. Phys*. **1983**, *78*, 4400.
(14) Yamashita, K.; Morokuma, K. *J. Chem. Phys*. **1990**, *93*, 3716.
(15) Vincent, M. A.; Connor, J. N. L.; Gordon, M. S.; Schatz, G. C. *Chem. Phys. Lett.* **1993**, *203*, 415.
(16) Visscher, L.; Dyall, K. G. *Chem. Phys. Lett*. **1995**, *239*, 181.
(17) González, M.; Hijazo, J.; Novoa, J. J.; Sayós, R. *J. Chem. Phys*. **1998**, *108*, 3168.
(18) Cohen, M. J.; Willetts, A.; Handy, N. C. *J. Chem. Phys*. **1993**, *99*, 5885.
(19) Bondi, D. K.; Connor, J. N. L.; Manz, J.; Römelt, J. *Mol. Phys*. **1983**, *50*, 467.
(20) Persky, A.; Kornweitz, H. *J. Phys. Chem*. **1987**, *91*, 5496.
(21) Kornweitz, H.; Broida, M.; Persky, A. *J. Phys. Chem*. **1989**, *93*, 251.
(22) Kneba, M.; Wolfrum, J. *Annu. Rev. Phys. Chem*. **1980**, *31*, 47.
(23) Schatz, G. C.; Amae, B.; Connor, J. N. L. *J. Phys. Chem*. **1988**, *92*, 3190.
(24) Garrett, B. C.; Truhlar, D. G. *J. Phys. Chem*. **1991**, *95*, 10374.
(25) Page, M.; McIver, J. W. *J. Chem. Phys*. **1988**, *88*, 922.
(26) Miller, W. H.; Handy, N. C.; Adams, J. E. *J. Chem. Phys*. **1980**, *72*, 99.
(27) Jackels, C. F.; Gu, Z.; Truhlar, D. G. *J. Chem. Phys*. **1995**, *102*, 3188.
(28) Kraka; E.; Dunning, T. H. In *Advances in Molecular Electronic Structure Theory*; AI: New York, 1990; Vol. I.
(29) Garrett, B. C.; Truhlar, D. G. *J. Am. Chem. Soc*. **1979**, *101*, 4534.
(30) Truhlar, D. G.; Isaacson, A. D.; Garrett, B. C. In *The Theory of Chemical Reactions*; Baer, M., Ed.; Chemical Rubber: Boca Raton, FL, 1985; Vol. 4.
(31) Garrett, B. C.; Lynch, G. C.; Allison, T. C.; Truhlar, D. G. *ABCRATE*, version 10; University of Minnesota: Minneapolis, MN, 1997.
(32) Corchado, J. C.; Chuang, Y. Y.; Fast, P. L.; Villá, J.; Coitiño, E. L.; Hu, W. P.; Liu, Y. P.; Lynch, G. C.; Nguyen, K.; Jackels, C. F.; Gu, M. Z.; Rossi, I.; Clayton, S.; Melissas, V.; Steckler, R.; Garrett, B. C.; Isaacson, A. D.; Truhlar, D. G. *POLYRATE*, version 7.8.1; University of Minnesota: Minneapolis, MN, 1997.
(33) Natanson, G. A.; Garrett, B. C.; Truong, T. N.; Joseph, T.; Truhlar, D. G. *J. Chem. Phys*. **1991**, *94*, 7875.
(34) Chuang, Y. Y.; Truhlar, D. G. *J. Phys. Chem. A* **1997**, *101*, 3808.
(35) Garrett, B. C.; Truhlar, D. G. *J. Chem. Phys*. **1984**, *81*, 309.
(36) Garrett, B. C.; Truhlar, D. G.; Grev, R. S.; Magnuson, A. W. *J. Phys. Chem*. **1980**, *84*, 1780.
(37) Liu, Y. P.; Lynch, G. C.; Truong, T. N.; Lu, D. h.; Truhlar, G. G.; Garrett, B. C. *J. Am. Chem. Soc*. **1993**, *115*, 2408.
(38) Liu, Y. P.; Lu, D.h.; González-Lafont, A.; Truhlar, D. G.; Garrett, B. C. *J. Am. Chem. Soc*. **1993**, *115*, 7806.
(39) Schatz, G. C.; Amae, B.; Connor, J. N. L. *J. Chem. Phys*. **1990**, *93*, 5544.
(40) Klein, F. S.; Persky, A.; Weston, R. E. *J. Chem. Phys*. **1964**, *41*, 1799.
(41) Kneba, M.; Wolfrum, J. *J. Phys. Chem*. **1979**, *83*, 69.